International Symposium of Research Students on Materials Science and Engineering
December 20-22, Chennai, India
Department of Metallurgical and Materials Engineering, Indian Institute of Technology Madras

THE STRUCTURAL AND OPTICAL STUDY OF InGaN/GaN MULTIPLE QUANTUM WELLS

J. C. Zhang, [a) *] **J. F. Wang,** [a, b)] **J. Chen,** [a)] **T. Dai,** [c)] **Q. Sun,** [a)] **Q. J. Jia,** [d)]
Y. T. Wang, [a)] **and H. Yang** [a)]

a) State Key Laboratory on Integrated Optoelectronics,
b) Institute of Semiconductors, CAS, Beijing 100083, China.
[b)] Department of Physics, Wuhan University, Wuhan 430072, China
[c)] Beijing laboratory of Electron Microscopy, Institute of Physics, CAS, Beijing 100083, China
[d)] Beijing Synchrotron Radiation Facility, Institute of High Energy Physics, CAS, Beijing 100039,China

ABSTRACT

The influence of dislocation and interface roughness on optical properties of InGaN/GaN multiple quantum wells (MQWs) is investigated by X-ray diffraction (XRD), transmission electron microscopy (TEM) and temperature-dependent photoluminescence (PL) spectroscopy. A simple method is presented to measure the mean dislocation density of MQWs by XRD. The results indicate dislocations, especially the edge type, act as nonradiative recombination centers in InGaN/GaN MQWs. At the same time both interface roughness and dislocations can broaden the PL FWHM, while the effect of the latter is evident only under low-interface-roughness condition.

Key words: InGaN/GaN Multiple Quantum Wells; Interface Roughness; Dislocation; Metalorganic Chemical Vapor Deposition (MOCVD); Photoluminescence

1. INTRODUCTION

InGaN thin films and MQWs are widely used as active layers in GaN-based light-emitting devices and laser diodes because it is possible to tune the optical band gap from visible to ultraviolet spectral range by changing the In composition.[1-3] Several groups reported that dislocations were nonradiative recombination centers in GaN and InGaN films. [4-6] In InGaN/GaN MQWs, however, the role of dislocations has not been clarified, though highly efficient blue/green light emitting diodes made of InGaN quantum well structure have been fabricated directly on a sapphire substrate in spite of a high dislocation density originating from a large lattice mismatch between GaN and sapphire substrate. [7, 8] The dislocation density can be measured directly by transmission electron microscopy (TEM), which, however, is time consuming, destructive and of limited statistical significance. X-ray diffraction (XRD) technology is high-resolution and nondestructive, with no need for special sample preparation or a special sample environment. These advantages make XRD an important and convenient method to assess crystal quality. Using the kinematical or dynamical theory, the characteristic structural parameters of multiple quantum wells (MQWs), including periodicity, period number, well or barrier thickness, composition and strain, can be obtained from the simulation of the double-crystal X-ray diffraction (DCXRD) or triple-axis X-ray diffraction (TAXRD). [9, 10] But in real MQWs, there are many structural defects, such as misfit dislocation, interface roughness and fluctuation of periodicity, which not only decrease the diffraction intensity but also broaden the satellite peaks. [11-13] The general DCXRD cannot distinguish these defects in GaN-related materials because the DCXRD curve is just the combination of those of $\omega/2\theta$ scan and ω scan. However, TAXRD can do because it is high-resolution. Interface roughness would broaden the

ω/2θ-scan satellite peaks, while dislocations broaden the ω-scan peaks. Interface roughness can be assessed by analyzing the dependence of satellite peak width on their orders. [14] To our knowledge, there is no report on measuring the dislocation density of MQWs to this day. In this work the dislocation density of MQWs were measured by TAXRD. Associated with photoluminescence (PL) the influence of dislocations and interface roughness on the optical properties in InGaN/GaN MQWs was studied.

2. EXPERIMENTAL

$In_xGa_{1-x}N$/GaN MQWs samples marked as A-G with different growth conditions grown by metalorganic chemical vapor deposition (MOCVD) were investigated in this paper. Before MQWs were grown, a thin low-temperature GaN buffer layer was deposited on (0001) sapphire then a 1.5-μm thick high-temperature undoped GaN epilayer followed by a 2-μm thick high-temperature n-GaN was deposited. Finally, about 30-nanometer GaN was deposited on the MQWs structure. The sample A has five periods and others have 10 periods. The In compositions were obtained by simulation of TAXRD and listed in table I. The diffraction patterns were performed on a triple-axis x-ray diffractometer (JPN Rigaku SLX-1A) and Beijing Synchrotron Radiation Facility. Temperature-dependent PL spectra were measured using a 325-nm He Cd laser as the excitation source. TEM measurements were carried out by a Philips cm200 FEG operating at 200kV

3. RESULT AND DISCUSSION

Figure 1 shows (a) (0002) symmetric and (b) $(10\bar{1}2)$ skew symmetric TAXRD patterns of all the samples. According to the kinematical theory, under symmetric diffraction condition the relationship of periodicity Λ with the angle spacing $\Delta\theta_M$ between adjacent peaks can be expressed: [15]

$$\Delta\theta_M = \frac{\lambda}{2\Lambda\cos\theta_B} \qquad (1)$$

where λ and θ_B are X-ray wavelength and Bragg angle of substrate, respectively.

In real MQWs, interface roughness would broaden satellite peaks except for the so-called zero order one. If the interface roughness is described by a Gaussian distribution function with standard deviation σ, the FWHM of the nth peak will be expressed: [14]

$$W_n = W_0 + (\ln 2)^{1/2} n\Delta\theta_M \cdot \frac{\sigma}{\Lambda} \qquad (2)$$

where n is the order of satellite peak and σ/Λ is the interface roughness. W_n and W_0 are the FWHMs of zero and nth order peaks, respectively. Dislocations broaden the satellite peak width in reciprocal space mapping along q_y, which is independent of satellite order. The dislocation density ρ can be calculated using the formula: [16]

$$\rho = \frac{\beta^2}{4.35\vec{b}^2} \qquad (3)$$

where $\vec{b}$ is Burgers vector and β stands for the FWHM of ω scan of every satellite peak.

The interval angle spacing of satellite peaks can be obtained from Fig. 1. According to formula (1), the periodicity of every sample has been calculated, as listed in table I.

The dependence of satellite peak FWHM on the satellite order is shown in Fig. 2. The dependence shows a linear relationship and sample A has the largest slope coefficient, while

those of B and D are approximately equal to C and E, respectively. According to formula (2), the interface roughness has been calculated from the slope coefficient of linear fit curve and listed in table I.

Figure 3 shows cross-sectional TEM weak-beam images of MQWs of sample D taken with different reflection vectors: (a) **g** =0002 and (b) **g** =$11\bar{2}0$. Fig. 2 (c) is the TEM cross-sectional image with higher magnification. The inset of Fig. 2 (b) is the corresponding electron diffraction pattern. It can be seen that most part of dislocations of GaN underlying layer penetrated through the MQWs. But due to the limitation of magnification, the details of the dislocations in MQWs were difficult to observe, and correspondingly the density was difficult to be measured accurately, especially in partly relaxed MQWs. In the case of magnified image of MQWs (the inset of Fig. s (c)), there were only one or two dislocations can be observed, which were difficult to distinguish the origin. From Fig. 2 (c) the interfaces are straight and there is no observable lateral fluctuation in the thickness. In addition, the periodicity fluctuation was very little. All the samples were grown at the control of computer and it is believed that the periodicity fluctuation should be similar. So the interface roughness is mainly due to the real interface roughness and the fluctuation of In composition of wells. The periodicity was about 23 nm obtained from the TEM image, which is consistent with the measurement of TAXRD.

There are three types of dislocations in group □-nitirdes: a ($\vec{b}_a = \frac{1}{3}<11\bar{2}0>$), c ($\vec{b}_c = \frac{1}{3}<0001>$) and $a+c$ ($\vec{b}_{a+c} = \frac{1}{3}<11\bar{2}3>$). If group □-nitirdes is grown along <0001>, the c type (including the c part of the $a+c$ type) dislocation density can be calculated from the FWHM of (0002) ω scan. At the same time a type (including the a part of $a+c$ type) dislocation density can be calculated from the $(11\bar{2}0)$-ω-scan FWHM. However, it is difficult to perform this diffraction and usually using other substitutes, such as $(10\bar{1}2)$ and $(11\bar{2}4)$ diffractions. But these diffractions also contain the contributions of c and $a+c$ type dislocations. So it needs to separate them.

The a+c type dislocation can be divided into a and c types. So here use 'edge dislocation' to represent the sum of pure a type and a part of $a+c$ type dislocation, and 'screw dislocation' to refer to the sum of pure c type and c part of $a+c$ type dislocation. In this approach, the c part and a part of $a+c$ type dislocation with the Burgers vectors vertical and parallel to [0001], respectively, are neglected.

If the diffraction vector $\vec{g}$ satisfies the conditions of both $\vec{g}\bullet\vec{b}=0$ and $\vec{g}\bullet\vec{b}\otimes\vec{l}=0$ ($\vec{l}$ is the dislocation line vector) except when the dislocation runs parallel to a high symmetry axis, the dislocation has no contribution to the FWHM β of ω scan. On the other hand, the value of β is proportional to $\vec{g}\bullet\vec{b}$.[17] If the x-ray rocking curve is assumed to be Gaussian in shape, the FWHM of $(10\bar{1}2)$ ω scan can be written as $\beta_{(10\bar{1}2)}^{\ 2} = \beta_s^{\ 2} + \beta_e^{\ 2}$, where β_s and β_e are the contributions of screw and edge dislocations to the FWHM of $(10\bar{1}2)$ ω scan. The dislocation density ρ can be calculated using formula (3). For screw dislocation,

$$\rho = \frac{\beta_{(0002)}^{\ 2}}{4.35\vec{b}_c^{\ 2}} = \frac{\beta_s^{\ 2}}{4.35\vec{b}_{cc}^{\ 2}}$$

where $\vec{b}_{cc}$ is the part of $\vec{b}_c$ contributing to the FWHM of ($10\bar{1}2$) ω scan and $\left|\vec{b}_{cc}\right| = \left|\vec{b}_c\right| \cos 43.189^{\mathrm{O}}$. So the edge dislocation density can be also calculated.

The ω scan of every satellite peak of ($10\bar{1}2$) as well as (0002) diffraction has been performed. The screw and edge dislocation density have been calculated and listed in table I. Theoretically, the mosaic spread can result in the increase broadening of the ω scan FWHM as the order increase from the higher negative satellites to higher positive ones. However, this phenomenon was not found in this experiment. All the FWHMs deviated less than 5% and the deviation was irregular. So in this work, the influence of Mosaic spread was very little, consistent with the experiment result of Ref. 18, whose growth system is the same as this work. As another factor, the indiffusion does not influence the FWHM of the satellite and only decreases the intensity of satellite, especially the higher order ones. Wafer bending or heterogeneous strain also does not influence the peak broadening owing to the small acceptance angle of the detector.

Figure 4 shows the dependence of PL integrated intensity on total dislocation density of all the samples except A, which has 5 periods and its PL intensity does not compare with others. The inset shows the influence of edge and screw dislocation density on PL intensity, respectively. It is well known that PL intensity of □-nitrides decreased with increase of wavelength. But in this work the PL intensity of sample B, C, D and G increase with the increase of wavelength, just opposite to this knowledge. Though the intensity of sample E is about twice less than that of sample D, according to Ref. 19 the efficiencies in the wavelength range of sample D and E (440- 455 nm) do not change only due to varying wavelength, while according to Ref. 20 the efficiencies decrease only 9%, which is far less than the values of this work. So there must be other factors to influence the PL intensity. From Fig. 4, it can be seen that PL intensity decreases with the increase of total dislocation density, which suggests that dislocations act as nonradiatve recombination centers in InGaN/GaN MQWs. It is noticed from the inset that screw and edge dislocations have different effects on the PL property. The dependence of PL intensity on screw dislocation is irregular, while the dependence on edge dislocation density has the same trend as that on the total dislocation density, indicating that the influence of edge dislocations on PL intensity should be more important than that of screw dislocations. The experimental results suggest that the reduction of dislocation density, especially the edge dislocation density, is essential to increase the PL intensity, which is undoubtedly beneficial to improve the performance of laser diodes or light-emitting diodes composed of InGaN/GaN MQWs.

Figure 5 shows the Arrhenius plots of all the samples. The inset is the temperature-dependent PL of sample G. The activated energy of the thermal quenching of PL intensity can be obtained and listed in table I. In a compound semiconductor, the energy fluctuation can localize excitons. The activation energies represent the localization energies of the localized excitons in the InGaN quantum wells. The localized exciton emission linewidth is also induced by the energy fluctuations in the band edge due to the In composition fluctuation, which should then be of the same order as the exciton localization energy. [21, 22] However, all of the room-temperature (RT) PL FWHMs were larger than the sum of In-composition-fluctuation-induced broadening and the thermal broadening (considering the Gaussian shape of PL peak).

Figure 6 (a) shows the dependence of the RT PL FWHM on interface roughness. The FWHM

trends to increase as the interface roughness increase, but at the condition of less than 7%, it seems zigzag. It was reported the FWHM increased as the In composition increased. [23, 24] In this work the samples C and D, E and G have similar composition, respectively. It can be seen that as the interface roughness increased, the FWHM also increased. The least composition of sample F is at least one of the reasons responsible for the smallest PL FWHM. Sample A has the largest value. According to the Ref. 24, whose growth system is the same as that used in this work, the difference of A and E (or G) should be less than 1 nm. Even according to the Ref. 23 the difference should be less than 15 nm. However, the experimental difference is about 47 nm (0.2423 eV). So it is believed the large interface roughness is the reason. From this figure it can be also seen that the results seems to contrary to the references because the FWHM of sample B is the second largest one and its composition is not the second largest, at the same time, its interface roughness is similar to that of sample C. There must be some reasons responsible for this. The dependence of the FWHM on the dislocation density is plotted in Fig.6 (b). As the dislocation density increased, the FWHM increase zigzag. The reason that samples E and G deviated slightly from the trend is perhaps their large In compositions. So it is the dislocation that answers for the larger FWHM of sample B than that of sample C. In addition, according to the Ref. 23 and 24, the difference of D and E should be less than 3 and 1 nm, respectively. However, in this work, the difference is about 4.0 ± 0.2nm (0.0190 eV). At the same time, the interface roughness of D is similar to that of E. So the reason should be the dislocation density of E is larger than that of sample C. Fig. 6 (b) exhibits that when dislocation density was more than 3.6×10^9 cm^{-2}, the FWHM increased sharply. Most probably this is due to the large interface roughness of near 46% shown in Fig. 6 (A). So both interface roughness and dislocations can broaden the FWHM of PL peaks. But when interface roughness is less than 7% in this work, the FWHM is mainly dependent on dislocation density.

4. SUMMARY

The influence of dislocation and interface roughness on optical properties of InGaN/GaN MQWs was investigated. Due to the limitation of the amplification, the dislocation density of the MQWs was difficult to be obtained by TEM measurements. A simple method was used to evaluate the dislocation density by XRD. The interface roughness was obtained by the dependence of the FWHM of satellite peaks on the peak orders. The TEM measurements showed the fluctuation of period of the MQWs was very little, so the interface roughness measured by TAXRD was mainly due to the real interface roughness and the fluctuation of the In composition of the wells. The contribution of the In composition fluctuation to the FWHM of RT PL was evaluated by thermal quenching of the PL intensity. The results show both interface roughness and dislocation can broaden the PL FWHM, while the effect of the dislocation is evident only under the low-interface-roughness conditions. At the same time, it is found that the dislocations act as nonradiative recombination centers, in which the edge dislocation is the decisive element to decrease RT PL intensity.

5. ACKNOWLEDGEMENTS

This work was supported by National Natural Science Foundation of China (No.69825107) and NSFC-RGC Joint Program (No.5001161953 and N-HKU028/00).

6. REFERENCES

1. A. F. Wrigh and J. S. Nelson, Appl. Phys. Lett. **66,** (1995) 3051
2. M. D. McCluskey, C. G. Van de Walle, C. P. Master, L. T. Romano, and N. M. Johnson, Appl. Phys. Lett.**72**, (1998) 2725
3. S. P ereira , M. R. Correia, T. Monteiro, E. Pereira, E. Alves, A. D. Sequeira, and N. Franco, Appl. Phys. Lett.**78**, (2001) 2137
4. S. J. Rosner, E. C. Car, M. J. Ludowise, G. Girolami and H. I. Erikson, Appl. Phys. Lett.**70**, (1997) 420
5. T. Sugahara, H. Sato, M. Hao, Y. Naoi, S. Kurai, S. Tottori, K. Yamashita, K. Nishino, L. T. Romano and S. Sakai, Jpn. J. Appl. Phys. **37**, (1998) L389
6. J. S. Speck and S. J. Rosner, Physica B **273-274**, (1999) 24
7. S. Nakamura, Science **281**, (1998) 956
8. T. Mukai, H. Narimatsu and S. Nakamura, Jpn. J. Appl. Phys. **37**, (1998) L479
9. Speriosu V S and Vreeland T, J. Appl. Phys. **56** (1984) 1591
10. Vandenberg J M, Hamm R A, Panish M B, and Temkin H, J. Appl. Phys. **62** (1987)1278
11. Auvray P, Baudet M, and Regreny A, J. Appl. Phys. **62** (1987)456
12. Hollanders M A and Thijsse B J, J. Appl. Phys. **70** (1991) 1270
13. He X and Razeghi M, J. Appl. Phys. **73** (1993) 3284
14. Pan Z, Wang Y T, Zhang Y, Lin Y W, Zhou Z Q, Li L H, Wu R H, and Wang Q M., Appl. Phys. Lett. **75** (1999) 223
15. D.KEITH Bowen and Brian K. Tanner, High Resolution X-ray Diffractometry and Topography (T.J.International Ltd, Padstow, 1998) p64
16. C. G. Dunn and E. F. Koch, Acta Met. **5**, (1957) 548
17. V. M. Kaganer, R. Kohler, M. Schmidbauer, R. Opitz, and B. Jenichen, Phys. Rev. B **55**, (1997) 1793
18. E.J.Thrush, M.J.Kappers, P.Dawson, M.E.Vichers, J.S.Barnard, G.Graham, F.D.G..Rayment, L.Considine, J.T.Mullins, C.J.Humphreys, Downloaded from www.msm.cam.ac.uk/GaN
19. M.Poschenriede, F.Schulze, J.Blasing, A.Dadgar, A.Diez, J.Christen, and A.Krost, Appl. Phys. Lett. **81**, (2002 1591
20. R.W.Martin, P.R.Edwards, R.Pecharroman-Gallego, C.Liu, C.J.deatcher, I.M.Watson, and K.P.O'Donnell, J. Phys. D **35**, (2002) 604
21. M.Smith, G.D.Chen, J.Y.Lin, H.X.Jiang, M.Asif Khan and Q.Chen Appl.Phys. Lett. 69, (1996) 2837
22. S.Chu, T.Saisho, K.Fujimura, S.Sakakibara, F.Tanoue, K.Ishino, A.Ishida, H.Harima, Y.Oka, K.Takahiro, Y.Chen, T.Yao and H.Fujiyasu. Jpn. J. Appl. Phys. **38**, (1999), 4973
23 S. Nakamura, M. Senoh, N. Iwasa, S. Nagahama Jpn. J. Appl. Phys. **34**, (1995), L797
24. E. J. Thrush, M. J. Kappers, P. Dawson, D. Graham, J. S. Barnard, M. E. Vickers, L. Considine, J. T. Mullins, and C. J. Humphreys, Phys. Stat. Sol. (a) **192**, (2002) 354

TABLES

TABLE1. Characteristics of MQWs including periodicity, composition, interface roughness, activated energy, screw and edge dislocation density.

Sample	Periodicity (Å)	Composition X_{In}	Interface roughness (%)	Screw dislocation density (10^8 cm^{-2})	Edge dislocation density (10^8 cm^{-2})	Activated Energy (meV)
A	113	0.16 ± 0.01	46 ± 5	11.1 ± 1.1	24.9 ± 2.5	119.6 ± 5.9
B	168	0.09 ± 0.01	6.7 ± 0.7	6.5 ± 0.7	22.5 ± 2.3	57.5 ± 5.9
C	173	0.11 ± 0.01	7.0 ± 0.7	6.1 ± 0.6	13.2 ± 1.3	29.3 ± 3.2
D	228	0.11 ± 0.01	4.0 ± 0.4	5.0 ± 0.5	6.3 ± 0.6	41.0 ± 4.1
E	220	0.14 ± 0.01	3.6 ± 0.4	8.0 ± 0.8	6.5 ± 0.7	30.6 ± 2.6
F	228	0.06 ± 0.01	5.0 ± 0.5	1.8± 0.2	3.4 ± 0.3	94.2 ± 12.9
G	220	0.14 ± 0.01	2.0 ± 0.2	1.6 ± 0.2	5.2 ± 0.5	72.2 ± 7.0

FIGURES

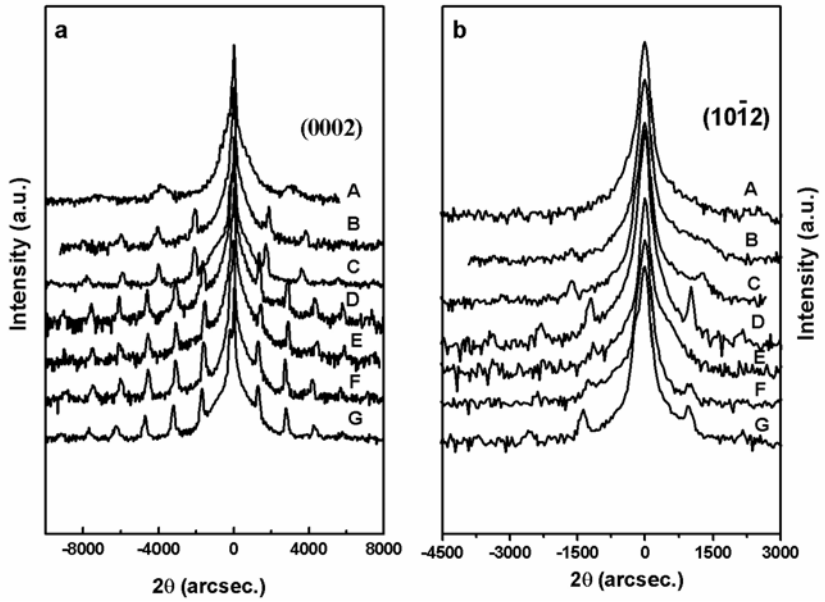

Figure 1. Triple-axis (0002) symmetric (a) and ($10\bar{1}2$) skew symmetric (b) ω/2θ diffraction profiles of all the InGaN/GaN MQWs.

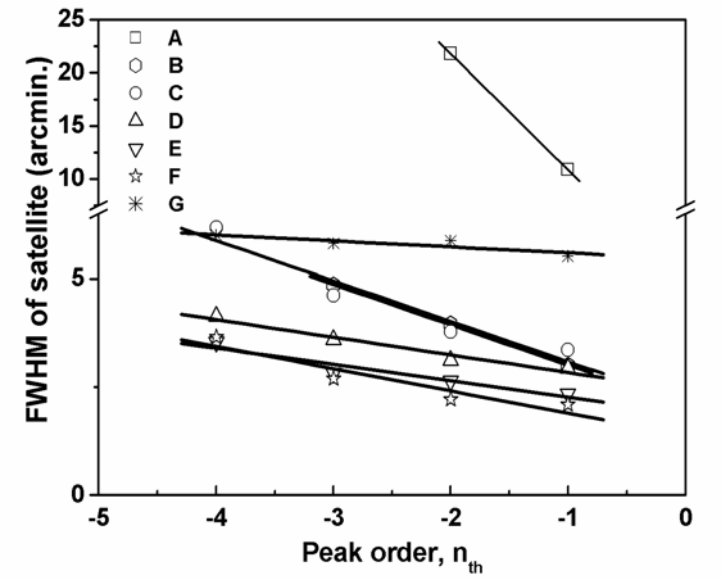

Figure 2. FWHM of satellite peaks vs peak orders in InGaN/GaN MQWs. Symbols and lines are experimental data and linear fit curves, respectively.

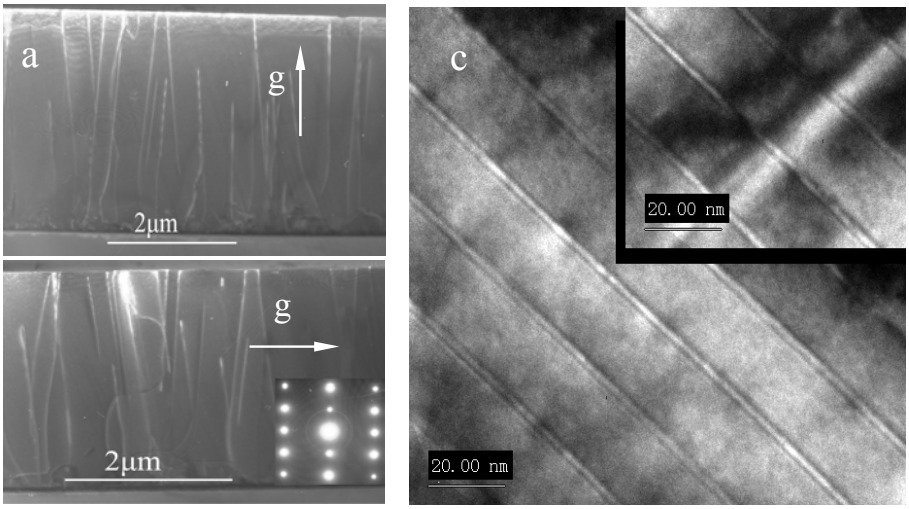

Figure 3. Cross-sectional TEM weak-beam images of MQWs of sample D taken with different reflection vectors at the same area: (a) **g** =0002 and (b) **g** =$11\bar{2}0$. c) TEM cross-sectional image with higher magnification. The insets of (b) and (c) are the corresponding electron diffraction pattern and a dislocation with higher magnification, respectively.

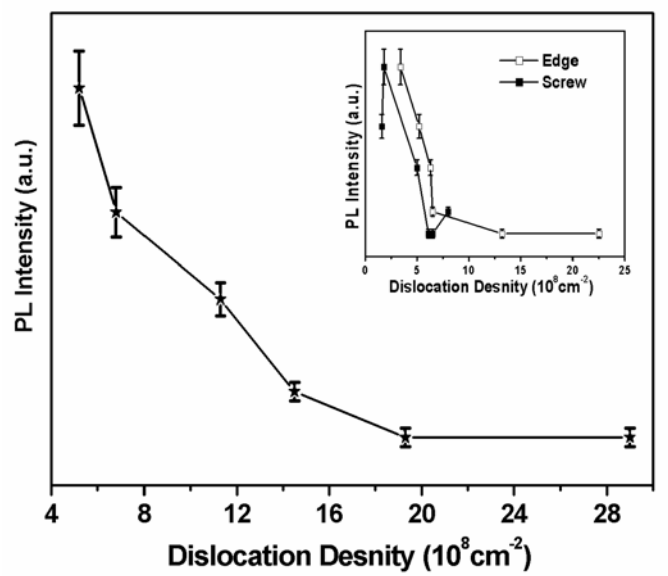

Figure 4. Dependence of PL integrated intensity on total dislocation densities. The inset shows the influence of edge and screw dislocation density on PL intensity, respectively.

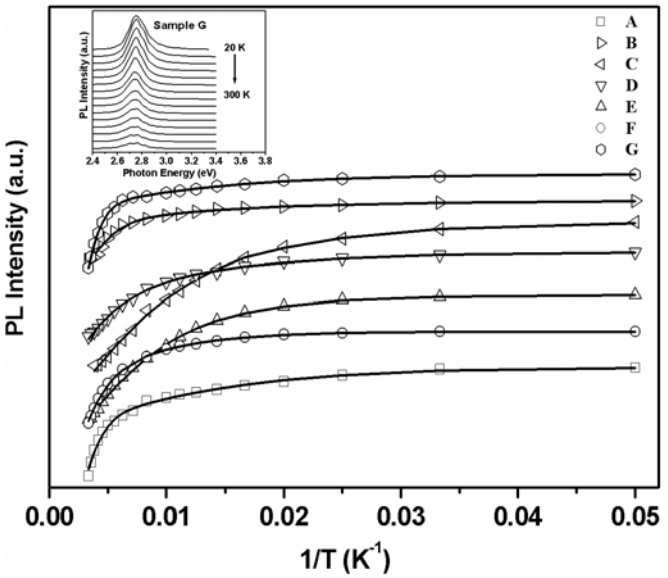

Figure 5. The Arrhenius plots of all the MQW samples. The inset is the temperature-dependent PL of sample G.

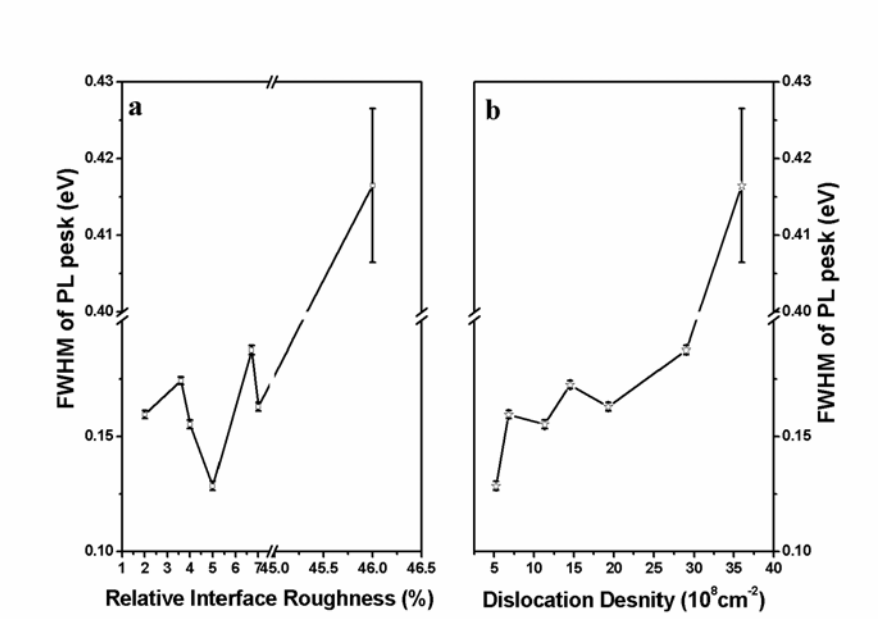

Figure 6. Dependence of the FWHM of RT PL peaks on interface roughness (a) and total dislocation density (b).